Int. J. Electrochem. Sci., 9 **(2014)** 1016 - 1032

International Journal of
ELECTROCHEMICAL
SCIENCE
www.electrochemsci.org

High Surface Area Tungsten Carbides: Synthesis, Characterization and Catalytic Activity towards the Hydrogen Evolution Reaction in Phosphoric Acid at Elevated Temperatures

Antonio Luis Tomas-Garcia, Qingfeng Li[*]*, Jens Oluf Jensen, Niels J. Bjerrum*

Department of Energy Conversion and Storage, Technical University of Denmark, Kemitorvet 207, DK-2800 Kgs. Lyngby, Denmark
[*]E-mail: qfli@dtu.dk

Received: 20 September 2013 / *Accepted:* 27 October 2013 / *Published:* 8 December 2013

Tungsten carbide powders were synthesized as a potential electrocatalyst for the hydrogen evolution reaction in phosphoric acid at elevated temperatures. With ammonium metatungstate as the precursor, two synthetic routes with and without carbon templates were investigated. Through the intermediate nitride route and with carbon black as template, the obtained tungsten carbide samples had higher BET area. In 100% H_3PO_4 at temperatures up to 185°C, the carbide powders showed superior activity towards the hydrogen evolution reaction. A deviation was found in the correlation between the BET area and catalytic activity; this was attributed to the presence of excess amorphous carbon in the carbide powder. TEM imaging and TGA-DTA results revealed a better correlation of the activity with the carbide particle size.

Keywords: tungsten carbide; synthesis; hydrogen evolution reaction, phosphoric acid

1. INTRODUCTION

For wide utilization of renewable energy sources e.g. hydropower, windmills or solar cells, a key issue is the effective energy storage technology over a shorter or longer time scale. Various types of technological scenarios are under consideration and active development. Hydrogen and its combination with the electrochemical energy conversion technology including fuel cells and electrolysers, have been well recognized as a reliable, secure and clean energy technology in association with renewable energy sources. One of the barriers for use of hydrogen as an energy carrier is the challenge of economic production of hydrogen. Water electrolysers, particularly proton

exchange membrane water electrolysers, provide a favorable and practical means of hydrogen production from the surplus electrical energy of renewable sources.

Great efforts are being made to develop highly active and sufficiently cost-effective catalysts for both electrodes of electrolysers. At the anode, where the oxygen evolution reaction (OER) takes place, the state-of-the-art catalysts in PEM electrolysers are based on IrO_2 or its composites with other oxides. For the hydrogen evolution, on the cathode side, platinum supported on active carbon (Pt/C) is widely used. There are large similarities between a hydrogen evolution electrode and a fuel cell electrode [1]. Due to the high price and low availability of noble metals, alternative catalysts are highly desired [1-3].

Transition metal carbides, particularly those of the group 6 metal elements, have long been known for their catalytic properties analogous to precious metals [4-7] and explored for both chemical [8] and electrochemical [9] applications. Of practical interest are tungsten carbides with stable phases of α-WC and W_2C. Earlier exploration of catalytic applications of WC was carried out on low surface area materials. The key to achieve better catalysis is to synthesize high surface area carbides.

Chemically WC can be prepared by carburization of tungsten metal, trioxide and tungstic acid or salts with a variety of carbon sources. Earlier efforts were well reviewed by Iglesia et al [10]. The commonly used carbon sources include carbon black, hydrocarbons and carbon monoxide (CO). Reactive vapor synthesis from e.g. WCl_6 and hydrocarbon mixtures led to non-stoichiometric products, apparently containing a large quantity of free carbon. Attempts were made to prepare high surface area tungstic acid precursors, which were then directly carburized in CO or reduced in hydrogen followed by carburization of the tungsten metal in CO [10]. The surface area of the thus obtained WC was steadily improved. However, the use of CO or CO/CO_2 mixture in the carburization of the tungsten metal results in an oxidative atmosphere and therefore residual oxygen in the carbide samples. When carbon black is used as a solid reducing agent, high temperatures above 1000 °C are necessary for the synthesis. As a result the product was usually a mixture of WC, W_2C, and metallic tungsten with some residual carbon. In term of electrochemical stability in acidic media, WC is more favorable than W_2C [11, 12].

The use of gaseous mixtures such as CH_4/H_2 as a reducing agent allows for a simultaneous reduction of tungsten oxides and carburization of the metal. In this way the elimination of oxygen and introduction of carbon are controlled independently. A significant advance was achieved by the so called temperature programmed reaction (TPR) method developed by Boudart et al. [10, 13] at Stanford University. With a hydrocarbon, typically methane or ethane, as the gaseous carbon source, tungsten trioxide is normally used as the tungsten source. By careful control of the temperature profile at a very slow ramp (typically lower than <0.01 °C/s), carburization of metal oxides under a flow of a methane/hydrogen mixture takes place forming porous carbides of high specific surface area. When an ammonia flow is applied as a nitriding agent instead of the methane/hydrogen mixture, W_2N powders of high surface area have also been successfully synthesized [14]. Further carburization of the obtained tungsten nitrides with methane/hydrogen mixtures led to formation of carbides that inherited the crystalline size and high surface area of the nitride intermediate. This is a typical topotactic reaction where the lattice of the parent crystal remains in the bulk solid of the product phase. The nitride-to-carbide transformation is achieved by diffusion of interstitial N and C atoms through the solid phase

with no rearrangement of the metal atoms in the entire lattice of the nitrides. In other words, the synthesis does not result in sintering of the particles or loss of the surface area, which otherwise always is a challenge for high temperature process.

Recent efforts, as reviewed by Antolini and Gonzalez [9], are being made to synthesize functional WC for proton exchange membrane fuel cells. Different approaches have been employed to produce high surface area carbides. Examples include the use of WO_3 nanoparticles [15], templates [16, 17] or carbon-tungsten composite precursors [18-21]. The motivation of these works is primarily threefold. They are expected to serve as synergistic supports for noble metal catalysts for ORR [22-25], though the susceptible instability of the carbide supports under fuel cell cathodic conditions has been a critical concern. Another potential use of the carbide is as either catalysts or catalyst supports for direct oxidation of small organic molecules [26]. The third possible application of the carbide is as catalysts for oxidation of hydrogen. For the last purpose the reported catalytic activity is inferior compared to platinum, but its low cost and superior tolerance to H_2S and CO make the materials potentially interesting [27, 28].

Very recently, Ham et al. [29] evaluated W_2C microspheres as catalysts for the hydrogen evolution reaction (HER) in sulfuric acid, apparently at room temperature. Of note are recent advances in PEM fuel cell and electrolyser technologies for operation at intermediate temperatures based on phosphoric acid doped polymer membranes [30] or inorganic phosphates [31]. In the present work high surface area tungsten carbide in a pure form of WC is synthesized and evaluated as catalysts for the hydrogen evolution reaction in phosphoric acid at elevated temperatures. Special attention is paid to the determination and effect of carbon inclusions.

2. EXPERIMENTAL

2.1. Sample preparation

2.1.1. Carburization routes

Two synthesis routes were used to prepare the tungsten carbide powders, as seen in Figure 1. In the first route, ammonium metatungstate (AMT) was first calcinated at 600 °C in an alumina boat in air for 5 h (Eq. 1). The obtained yellow tungsten oxide (WO_3) was then placed in a quartz tube oven under a flow of H_2 and CH_4 (80/20% v/v, 200 mL/min). The oven was heated at 8 °C/min up to 880 °C, holding the final temperature for 2 h (Eq. 2). The sample was finally cooled down to room temperature and referred to as WC-O.

$$(NH_4)_6H_2W_{12}O_{40}\cdot 5H_2O \rightarrow 12\ WO_3 + 6NH_3 + 9H_2O \quad (1)$$

$$WO_3 + CH_4 + H_2 \rightarrow WC + 3H_2O \quad (2)$$

The second route included an additional nitridization step. After the AMT calcination of the first route, the WO_3 was treated with pure ammonia (50 mL/min), applying a 5°C/min ramp up to 680°C, holding the final temperature for 2 h (Eq. 3). The obtained nitride was cooled down to room

temperature and then carburized under the same H_2 and CH_4 mixture as in the first route. The temperature ramp used for the carburization was 8°C/min up to 780°C, holding the final temperature for 2 h (Eq. 4). The carbide sample obtained via the second route is hereafter referred to as WC-N.

$$4WO_3 + 8NH_3 \rightarrow 2W_2N + 3N_2 + 12H_2O \quad (3)$$

$$2W_2N + 4CH_4 \rightarrow 4WC + N_2 + 8H_2 \quad (4)$$

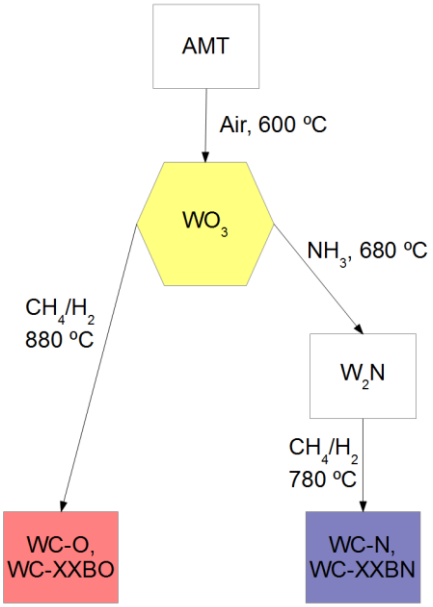

Figure 1. Reaction routes used for preparation of WC powders from ammonium metatungstate (AMT). Left: the oxide route where the obtained carbide was named WC-O. Right: the nitride route where the obtained carbide was named WC-N.

2.1.2. Carbon template impregnation

Carbon black was used as template with the goal of improving the texture properties of the WO_3 used for the carbide synthesis. The template used was commercial Vulcan® carbon black XC72R (Cabot Carbon Ltd). This carbon black has a BET area of ca. 250 m^2/g with predominance of meso- and micro- porosity. The impregnation method was as follows. 5 g of AMT was dissolved in 5 mL water. The carbon black was added to the solution until it soaked up all the liquid. This mixture was dried at 80°C overnight and then calcinated in air at 600°C for 5 h. AMT solutions of different concentrations were used for the impregnation of the carbon black, from 5% to 70% w/w. The concentration used for each sample can be found in Table 1. For each concentration, the obtained WO_3 was carburized either through the oxide route (the obtained carbide samples are hereafter referred to as WC XXBO) or the nitride route (the obtained carbide samples are hereafter referred to as WC XXBN). In both cases, XX is the initial AMT concentration in wt% for impregnation of carbon black.

2.2. Physical characterization

X-ray diffraction of the obtained powders was performed with a Huber G670 transmission diffractometer, using Cu K emission (1.54056 Å). The powders were deposited onto an adhesive polymeric tape, attached to a brass ring holder. The spectra were recorded with a resolution of 0.05° between 20 and 90°. The background signal of the adhesive tape was recorded and subtracted to the spectra prior to plotting.

Nitrogen adsorption at 77 K was used to determine the BET area of the samples. The setup used was a Micrometrics ASAP 2020 apparatus. The relative pressure interval for the BET area was between 0.05 and 0.25. Transmission Electron Microscopy (TEM) was used for imaging the texture of the samples. The powders were dispersed in ethanol for 30 min, and then dropped onto a Cu grid coated with carbon. The instrument used was a Tecnai T20 G2 S-TEM microscope.

Thermogravimetric analysis (TGA) was made using a Nietzsch STA 409 PC TG-DSC instrument. All samples were analyzed in air with a flow of 30 mL/min. The temperature program consisted of a 10 °C/min ramp from room temperature up to 800°C, with mass and differential thermal signals registered.

2.3. Electrochemical characterization

The electrochemical characterization of the samples was carried out in 100% H_3PO_4, which is thermally stable and allows an extension of the working temperature up to ca. 200 °C.

The polytetrafluoroethyene (PTFE) half-cell assembly is schematically represented in Fig. 2. A Teflon treated carbon paper (Toray H120) was first pre-coated with a smooth carbon (Vulcan® XC72R carbon black) layer of 1 mg C/cm^2 with PTFE as binder in a mass ratio of C/PTFE = 70/30 and cured at 365 °C for 20 min. The carbon paper was used as the electrode substrate, onto which a carbide containing ink was applied. The ink was made of the carbide powder, a 5% Nafion® dispersion and ethanol. Prior to coating the ink was ultrasonicated for at least 30 minutes. Thus prepared electrodes with carbide loading of about 1 mg/cm² were dried at 80 °C overnight. The electrode, with an active working area of 0.78 cm², was exposed to the electrolyte. Over the back side of the electrode was a flow of hydrogen (100 ml/min). The counter electrode was made of a spiral platinum wire fixed around the capillary tip of the reversible hydrogen reference electrode, which was situated on the top of the carbide layer. The whole cell was placed in an oven and the temperature was controlled at 185°C.

The protocol for electrochemical measurements included four steps. First, the cell was heated to the working temperature under a hydrogen gas flow through the back electrode chamber under the open circuit voltage (OCV) condition. Once the temperature was stabilized, 20 voltammetric cycles (CV) at 100 mV/s were performed between potentials of -0.2 and +0.2 V vs. RHE. Next, an electrochemical impedance spectrum (EIS) was measured at OCV in a frequency range between 10^4 and 10^{-2} Hz.

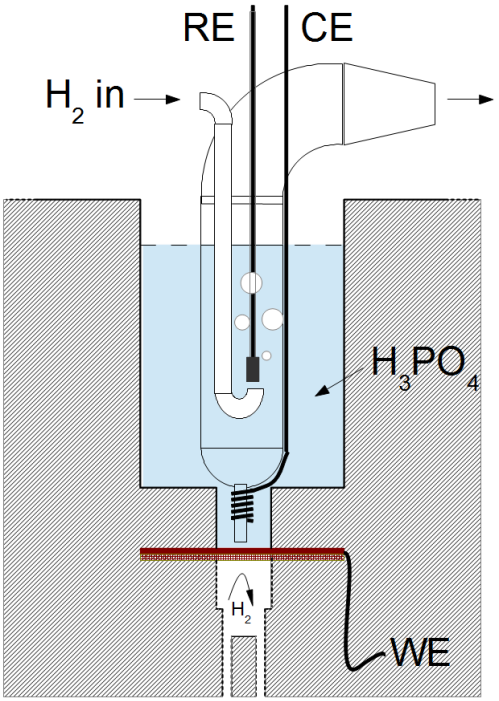

Figure 2. Schematic representation of the electrochemical cell used for the HER activity measurements.

Lastly, a staircase voltammetry experiment was performed between potentials of +0.2 and -0.2 V vs. RHE with a potential step of 10 mV in 30 s. This protocol was repeated for different temperatures. The ohmic resistance of the cell was determined from the real impedance at the frequency of 10^3 Hz and it is corrected to the staircase voltammetry measurements.

3. RESULTS AND DISCUSSION

3.1. Physical characterization

The XRD spectra obtained for all the samples obtained showed only the α-WC phase, without any other crystalline phase detected (Figure 3). This is in agreement with previous literature [32], showing the complete conversion of the reactants (WO_3, W_2N). In case of partial conversion, there would be other remaining intermediates, namely the reactant or subcarbides (WC_x). This seems to be the case when other gas mixtures are used, like pure CH_4 [13] or C_2H_4/H_2 [32], which were reported to favor the production of WC_x. Thus, according to the spectra, the two routes used in this study produced only α-WC.

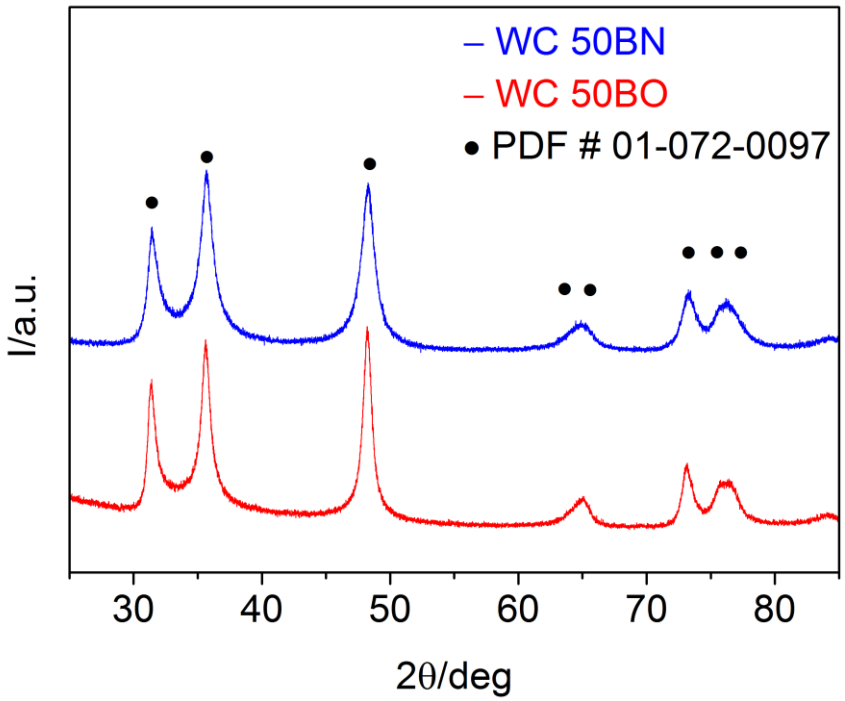

Figure 3. XRD spectra of WC powders obtained through both synthetic routes using a carbon black template. Red: sample made from 50% AMT via the oxide route. Blue: sample made from 50% AMT via the nitride route.

The results of the BET area calculations are listed in Table 1. First, two samples were prepared without the carbon black template through the direct carburization (WC-O) and through the nitride route (WC-N). The WC-N sample shows a higher surface area than that of the sample WC-O. This difference was also seen in the samples prepared with the Vulcan template, i.e., all samples prepared through the direct carburization route show lower surface areas than those of the samples prepared through the nitride route. This effect is in agreement with the observation of Hara et al. [15], where the increased surface area was attributed to different WC morphologies depending on the used precursor. In that work, where WC was prepared from a W_2N precursor, the general morphology was preserved. However, TEM imaging of the WC crystallites showed a pellet-like structure which was absent in the W_2N crystals. Thus, the surface area enhancement observed in the present study seems to come from the formation of these platelets. These structures were not observed in the case of the direct WO_3 carburization.

Figure 4 shows the relative increase in BET area when using carbon black impregnated with AMT solutions. It can be seen that, for the oxide synthesis route, a 10-fold increase in BET area is observed with respect to the sample prepared by the same method but without carbon black (sample WC-O). For the nitride route, an increase in BET area is also observed, although smaller, ca. 3 times more than the corresponding sample (WC-N). This indicates the positive effect of the presence carbon black in the final WC samples. The effect is most likely due to a smaller particle size for the WO_3

formed through calcination of AMT at 600°C. The area increase seems to be largely independent of the AMT solution used, within a wide concentration range (5-70% w/w).

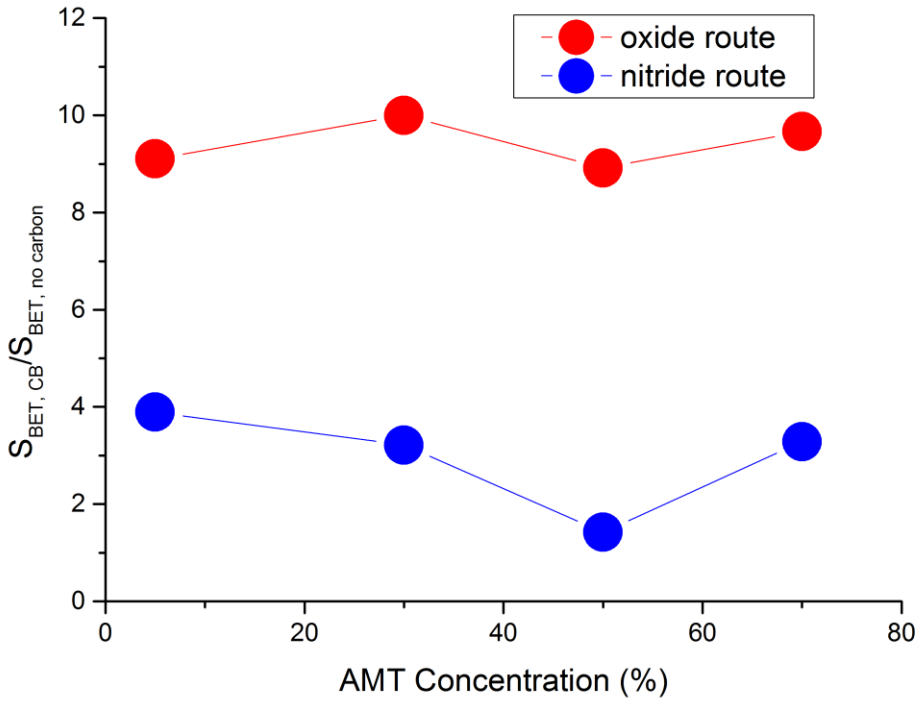

Figure 4. BET area improvement of WC samples with the use of carbon black template impregnated with AMT solutions of different concentrations.

TEM images of three materials are shown in Figure 5. The first sample was the WO_3 powder formed after the calcination of carbon black impregnated with the 50% AMT solution. The oxide particles have oblong shapes with sizes mostly in the 100-200 nm range. The second sample is WC prepared from the WO_3 through the direct oxide carburization route. Here, the carbide particles looked similar in size, although the shape was more cubic. The third picture shows WC prepared through the nitride carburization route. In this case, the particles were significantly smaller and with irregular shapes.

The difference in the WC morphology obtained via the two routes was apparently not inherited from the WO_3 precursor which initially was the same. In case of the oxide route, the particle size seemed to be inherited from the precursor, but in the nitride route, a new texture was developed. In addition, the samples seemed containing some free carbon, which showed better transmission than tungsten. This will be discussed in more detail in Section 3.3.

An analysis of the particle size distribution for the three powders is also shown in Figure 5. Although there was a significant spread in the particle diameters, the carbide prepared through the oxide route showed the similar size to the parent oxide. This small particle growth during the TPR process indicates that there was no considerable sintering during the carburization of the oxide. For the

nitride route, the particle size of the carbide product was significantly smaller than that for the oxide route.

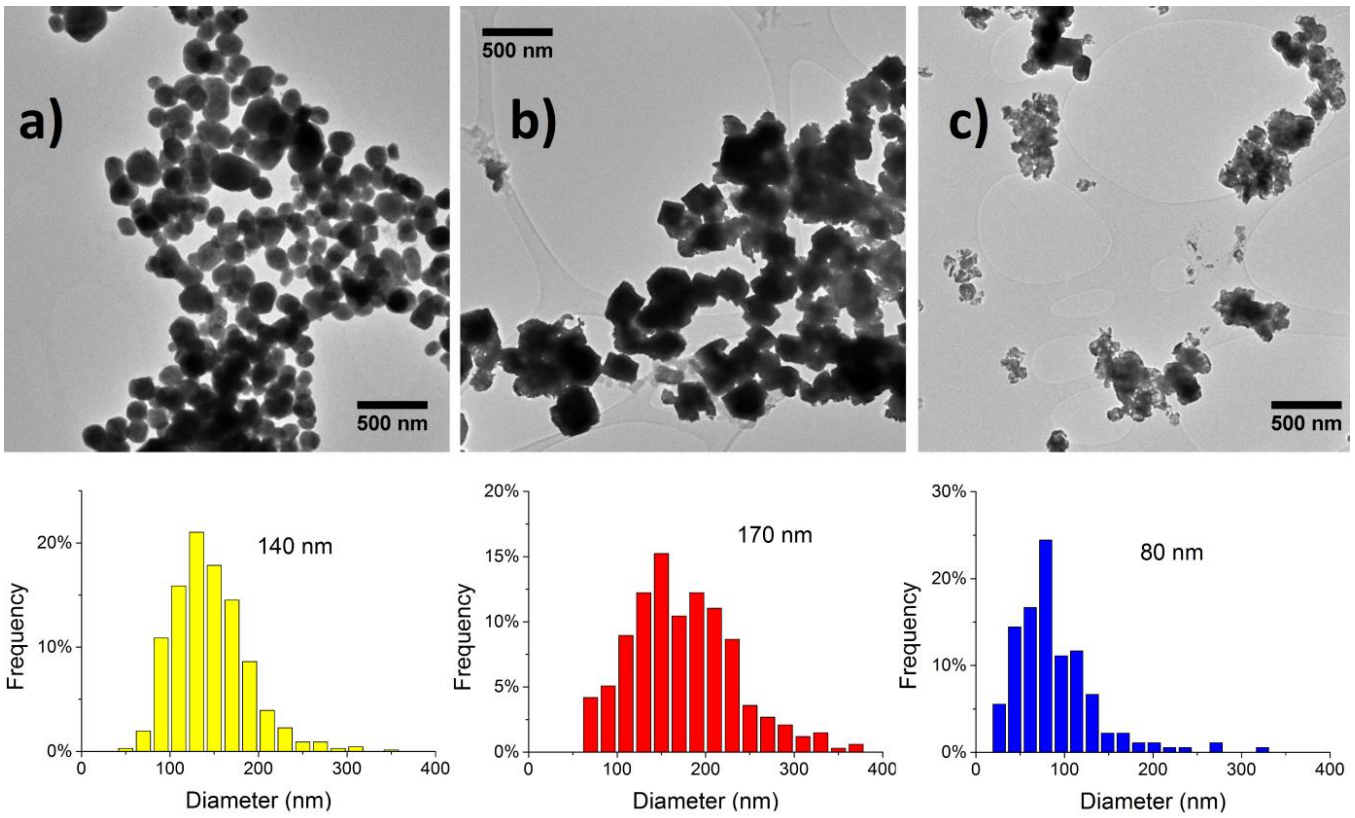

Figure 5. TEM images taken for different powders. a) WO_3 from 50% AMT impregnation. b) 50BO WC sample. C) 50BN WC sample. Bottom: Particle Size Distributions for each powder, measured from TEM images.

3.2. Electrochemical characterization

Cyclic voltammetric (CV) measurements of selected samples in H_2-saturated H_3PO_4 at 185°C are shown in Figure 6. A cathodic hydrogen evolution current was clearly seen while the corresponding hydrogen oxidation current was relatively small. This could be due to the insufficient diffusion across the carbon paper in the working electrode. As compared with the platinum electrodes (which was not shown but is well known from literature), there were no hydrogen adsorption peaks; instead, only a capacitive current was observed on top of the small hydrogen oxidation current, showing the weak hydrogen adsorption on the tungsten carbide. At the same time, no oxidation of the carbide at potentials of up to +0.2 V vs. RHE or other reduction current peaks at potentials <0 V vs. RHE were observed.

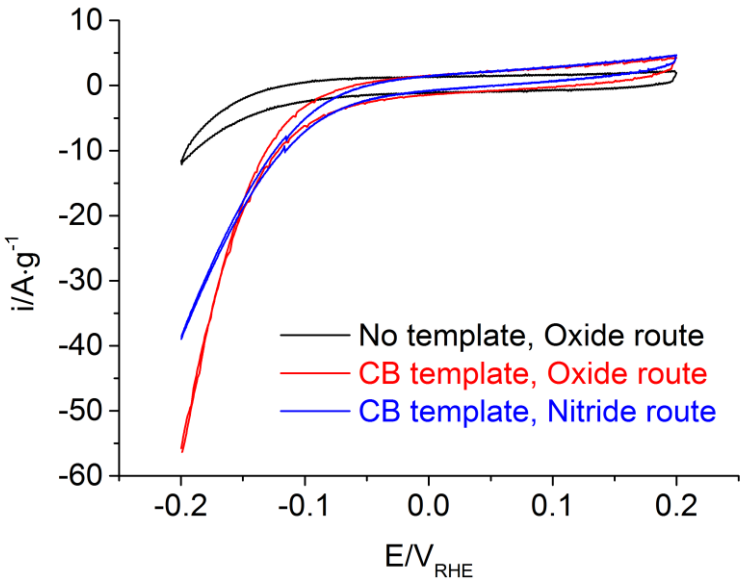

Figure 4. Cyclic voltammetric measurements for three samples. Scan rate 100 mV/s, 185 °C, H_3PO_4 100%.

The HER activity was measured for all samples. In addition to this, a background measurement was performed for the electrode substrate (carbon black + PTFE). No visible activity was measured for potentials above -0.2V vs. RHE at temperatures of up to 185 °C. Thus, the activity measured was attributed to the carbide samples. From the staircase voltammetry measurements, the i-V data were fitted to the Tafel equation:

$$\eta = \frac{2.303RT}{\alpha_C F}\log i_o - \frac{2.303RT}{\alpha_C F}\log i_o \qquad (5)$$

Figure 7 shows the experimental Tafel plots for several samples, with the potentials corrected for the ohmic loss. Even though the activities are different, it can be seen that the Tafel slopes are similar, which indicates that the HER mechanism is the same regardless of the synthesis route or whether the carbon black template was used in the WO_3 preparation. In Table 1 the obtained values for the Tafel equation fittings are listed. In general, for the samples prepared through the nitride route (WC-N, WC-XXBN) the observed activity was higher than that of samples prepared through the oxide route (WC-O, WC-XXBO). In principle, this would be due to the higher surface area obtained for the nitride route.

As seen from Figure 8, the nitride route samples in general showed higher activity than the oxide route samples. However, when the specific current density at -100 mV_{RHE} is plotted vs. the BET area (Figure 8) for all samples, a clear trend was not observed. In theory, the HER current should be proportional to the catalyst active area.

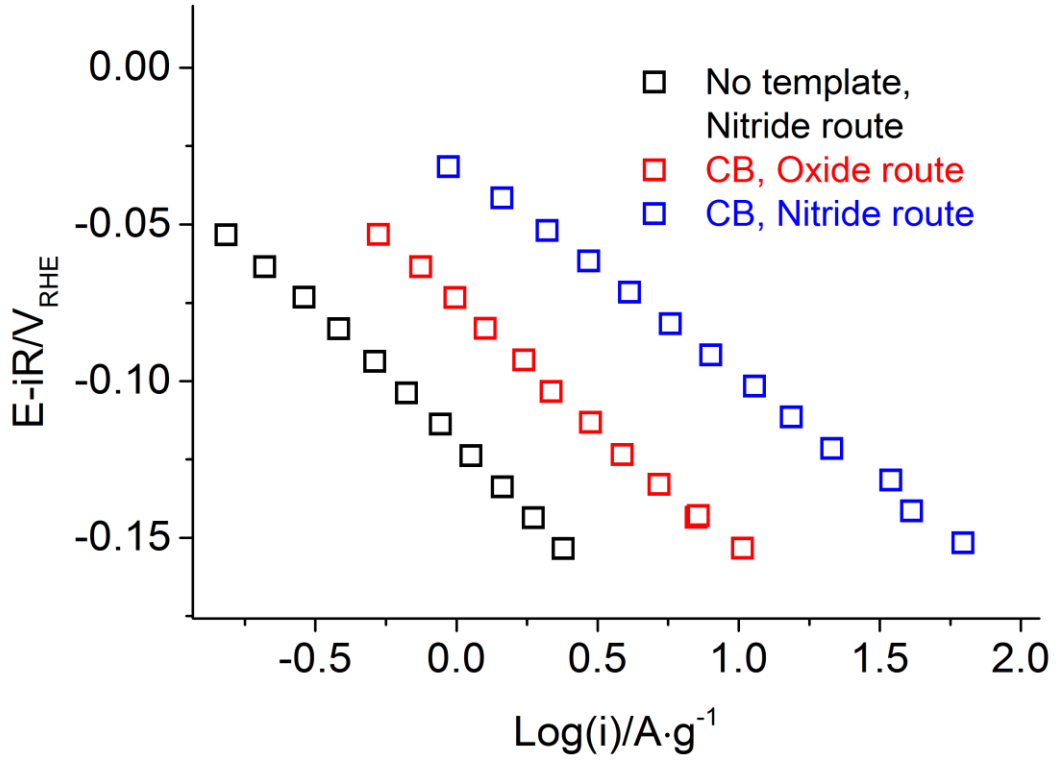

Figure 5. Tafel plots for selected WC samples. Measurements made at 185 °C in 100% H_3PO_4.

The voltammograms (Figure 6) showed no visible mass transport limitation for the HER branch, although different ohmic limitations were observed (corrected with AC impedance). A possible explanation for this issue was that the composition of the samples was not homogeneous, or in other words, the samples contained impurities. Chemical impurities could arise from contamination, or from imperfect synthesis. According to the XRD analysis, the only crystalline form obtained was the α phase. Taking this, as well as the synthesis temperatures and used reactants, into account, the most likely material to be formed in addition to the carbide phase was some kind of amorphous carbon. The chemisorption of CH_4 is the first step in the reaction [33]:

$$2W^* + CH_4 \rightarrow W_2CH_2^* + H_2 \qquad (6)$$

After dehydrogenation, the carbon atoms diffuse into the W precursor to form the carbide phase. Eventually, after the completion of the α-WC formation, more carbon could be deposited that could not diffuse into the material, thus accumulating as amorphous carbon. Amorphous carbon has a density of ca. 2 g/cm^3, which is significantly smaller than that of WC (15.7 g/cm^3 [34]), so a small amount of carbon formed could contribute significantly to the BET area of the material, especially if the carbon phase is porous.

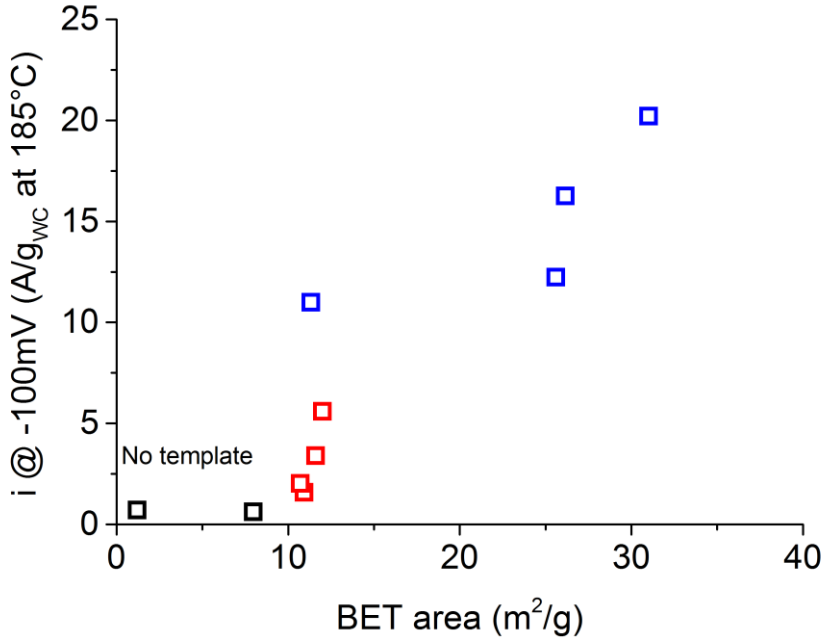

Figure 6. Specific current density of HER at -100 mV vs. RHE as a function of the BET area. Black: samples prepared without CB. Red: Samples prepared with CB through oxide route. Blue: Samples with CB were prepared through the nitride route. Measurements were made at 185 °C in 100% H_3PO_4.

In a recent study, Bosco et al. [17] prepared macroporous tungsten carbides using a polymer template and different synthesis routes. After thermogravimetric analysis of the samples, they found that the samples had BET areas depending on the carbon content, although in their case the carbon was a residue from the pyrolysis of the template. In one sample, they followed the direct carburization of WO_3, obtaining ca. 2.5% carbon excess. They found the WC particle size to be independent of the synthesis method, although they concluded that the presence of carbon was beneficial to the performance of the powders as catalyst supports for Pt. Even though the particle morphology and size was analyzed, there was no direct measurement of the carbide surface area.

3.3. Thermal analysis

Amorphous phases are hard to detect with XRD analysis. As discussed above, carbon formation could be a reason behind the poor correlation between BET area and activity. A way of determining the real composition of the samples is by thermogravimetric analysis. In this work, temperature programmed oxidation of the carbide samples in air was used. The prepared WC powders were placed in a TGA-DTA setup and heated under an air flow at 10 °C/min up to 800 °C. The mass, as well as the DTA signal, were registered for all samples.

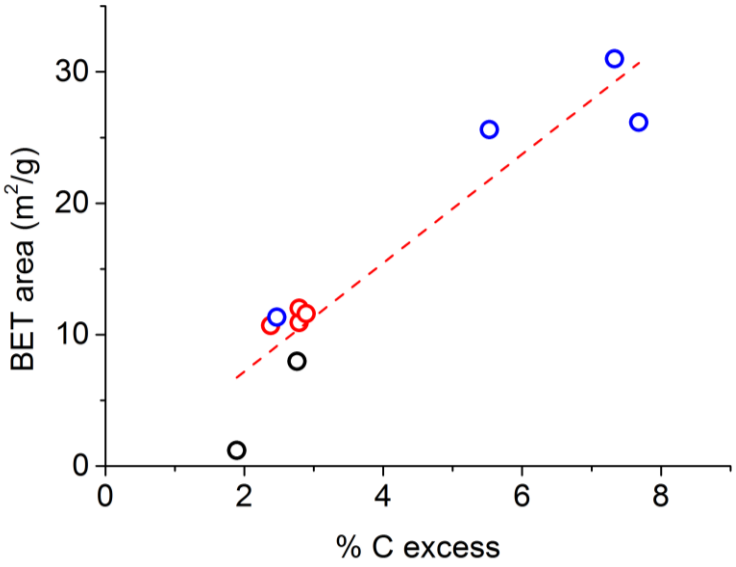

Figure 9. Evolution of the WC BET area with calculated carbon excess from the TGA experiments. Black: samples prepared without CB template. Red: samples prepared through the oxide route with CB template. Blue: samples prepared through the nitride route with CB template.

The sample composition was calculated from the final mass change. Assuming that there is only α-WC and elemental carbon in the fresh samples and the only solid combustion product is WO_3, the fraction of each phase can be determined:

$$WC_{(s)} + 5/2\ O_{2(g)} \rightarrow WO_{3(s)} + CO_{2(g)} \quad (7)$$

$$C_{(s)} + O_{2(g)} \rightarrow CO_{2(g)} \quad (8)$$

$$\%\ free\ C = 100 \cdot (1 - \frac{m_f}{m_i} \cdot \frac{MW_{WC}}{MW_{WO_3}}) \quad (9)$$

In Equation (9), m_i and m_f are the initial and final masses in the TGA experiment, respectively; MW_{WC} and MW_{WO_3} are the molecular weights of WC and WO_3, respectively.

The results of this calculation are summarized in Table 1. The fraction of free carbon ranges from ca. 2 to 8%. If different preparation methods are compared, it can be seen that the nitride route tends to produce higher amounts of free carbon than the oxide route. In Figure 9 we can see the dependence of the sample BET area on the carbon excess. Taking into account the considerations exposed above, there is a high probability that the differences in BET areas observed in these samples are partly due to the formation of carbon, not merely different surface areas of carbide particles. In fact, we could calculate the BET area of the amorphous carbon from the linear regression shown in Figure 9; the slope yields ca. 400 m^2/g-C. This value is not uncommon in carbon materials, especially carbon blacks. As shown in Figures 5 and 10, the particle size seems to be a better descriptor for the activity of the WC particles than the BET area measurements. The higher BET area observed for the nitride synthesis route compared to the oxide route must have then two contributions: the smaller

particle size obtained with the nitride route, and the higher amount of free carbon formed during the TPR treatment.

Table 1. Characterization results for the prepared samples.

Sample	Carbon black	Route	AMT concentr. (%)	S_{BET} (m^2/g)	m_{Tafel} (mV)	i_0 (A/g-$_{WC}$)	I (η=-100mV) (A/g-$_{WC}$)	free C %	DTA peak (°C)
WC-O	No	Oxide	70	1.21	77	0.04	0.71	1.89	547
WC-N	No	Nitride	70	8.0	89	0.05	0.62	2.76	539
WC-05BO	Yes	Oxide	5	10.9	80	0.09	1.58	2.79	585
WC-30BO	Yes	Oxide	30	12.0	77	0.3	5.6	2.79	526
WC-50BO	Yes	Oxide	50	10.7	74	0.09	2.0	2.38	536
WC-70BO	Yes	Oxide	70	11.6	70	0.13	3.4	2.89	554
WC-05BN	Yes	Nitride	5	31	69	0.7	20	7.33	443
WC-30BN	Yes	Nitride	30	26	69	0.4	12.2	5.53	483
WC-50BN	Yes	Nitride	50	11.3	68	0.4	11.0	2.47	497
WC-70BN	Yes	Nitride	70	26	73	0.7	16.3	7.68	448

However, there are significant differences in the activities of samples prepared from different methods. If the carbon formed is considered inert towards hydrogen evolution (compared to WC), there must be a difference in the carbide particles, either in surface catalytic properties, or in active surface area. Kurlov et al. [35] modeled the relationship between the DTA combustion peak temperature and the particle size for WC particles of known size distributions. According to the authors, the activation energy for the oxidation of WC to WO_3 is inversely proportional to the particle size. Since smaller particles have a higher surface area, the particles with higher surface area should react faster.

Now, by simple geometrical considerations, WC samples with smaller particles should have higher specific areas, and thus higher HER activities. By plotting the experimental HER activity vs. the DTA peak temperature (Figure 10), a more clear correlation is obtained than when the BET area is used (Figure 8). According to Kurlov et al., samples with lower peak temperature should have smaller particle size distributions. This in turn can explain the correlation between the activity and TGA peak temperature. Thus, it seems that the differences in activity for the prepared samples can be explained better in terms of particle size, rather than the BET area. And the reason for the discrepancy between BET area and particle size might be the presence of amorphous carbon in the prepared powders, which adds specific surface area, but not the HER activity.

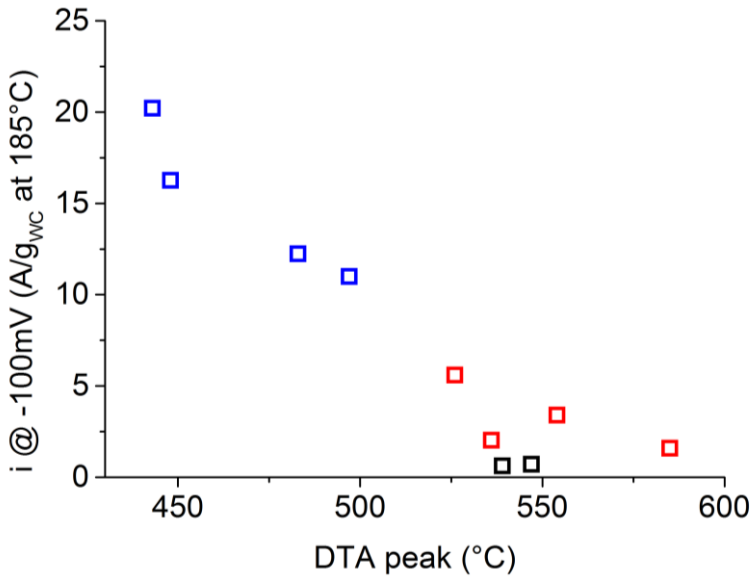

Figure 10. Specific HER activity of WC samples vs. TGA calcination peak temperature. Black: samples prepared without CB (WC-O and WC-N). Red: samples prepared with CB through oxide route (WC-XXBO). Blue: samples prepared with CB through nitride route (WC-XXBN). Measured at -100 mV polarization in H_3PO_4 100% at 185 °C.

Removal of the amorphous carbon has been proposed by post-synthesis treatment with H_2 at 700°C to gasify the elemental carbon [10, 36]. The hydrogen treatment or the carbon hydrogenation did not seem to alter the structure and crystal size of the carbide phase but was found to be able to restore the lost porosity during the carburization of the nitride precursor. Taken into account the carbon/methane equilibrium,

$$C_{(s)} + 2\ H_{2(g)} \rightarrow CH_{4(g)} \qquad (10)$$

it is possible in principle to completely remove the amorphous carbon. However, this treatment can also remove carbon from the *carbide* structure, thus partially reversing the carbide synthesis and altering its catalytic properties. A careful study of the optimum conditions for excess carbon removal would thus have to take into account the stability of the WC phase towards carbon re-gasification.

4. CONCLUSION

Tungsten carbide powders were prepared from two synthetic routes and evaluated as electrocatalysts for the hydrogen evolution reactions in acidic electrolytes at elevated temperatures. It was found that the indirect carburization of tungsten oxide through an intermediate nitride produced samples of higher BET area and HER activity than the carbide samples from the direct carburization of WO_3. When carbon black was used as a template for preparation of the WO_3 precursor, the final carbide powders can be tailored in terms of BET area and the electrochemical activity for hydrogen evolution. A deviation was found in the correlation between the BET area and HER activity and

attributed to the presence of excess amorphous carbon. Further efforts by the thermogravimetric analysis revealed a better correlation of the HER activity with the peak oxidation temperature of carbides, which in turn was related to the carbide particle size.

ACKNOWLEDGEMENTS
This work has received financial support from the Danish National Research Foundation (the PROCON Center) and the Danish ForskEL programme (Catbooster).

References

1. A.Rabis, P. Rodriguez and T. J. Schmidt, *ACS Catal.,* 2 (2012), 864-890
2. A.Brouzgou, S. Song and P. Tsiakaras, *Appl. Catal. B: Environ.,* 127 (2012) 371-388.
3. Z. Chen, D. Higgins, A. Yu, L. Zhang and J. Zhang, *Energ. Environ. Sci.,* 4 (2011) 3167
4. L. H. Bennett, J. R. Cuthill, A. J. McAlister, N. E. Erickson and R. E. Watson, *Science,* 184 (1974) 563-565.
5. L. F. Mattheiss and D. R. Hamann, *Phys. Rev. B,* 30 (1984) 1731-1738.
6. H. Tominaga and M. Nagai, *B. Chem. Soc. Jpn.,* 83 (2010), 1501-1503
7. R. B. Levy and M. Boudart, *Science,* 181 (1973) 547-549
8. H. H. Hwu and J. G. Chen, *Chem. Rev.,* 105 (2005), 185-212
9. E. Antolini and E. R. Gonzalez, *App. Catal. B-Environ.,* 96 (2010), 245-266
10. E. Iglesia, F. H. Ribeiro, M. Boudart and J. E. Baumgartner, *Catal. Today* , 15 (1992), 307-337
11. H. Chhina, S. Campbell and O. Kesler, *J. Power Sources,* 164, (2007) 431-440.
12. M. C. Weidman, D. V. Esposito, Y.-C. Hsu and J. G. Chen, *J. Power Sources,* 202 (2012), 11-17
13. L. Volpe and M. Boudart, *J. Solid State Chem. ,* 59, (1985), 348-356
14. L. Volpe and M. Boudart, *J. Solid State Chem. ,* 59 (1985), 332-347
15. Y. Hara, N. Minami, H. Matsumoto and H. Itagaki, *App. Catal. A: Gen.,* 332 (2007), 289-296.
16. R. Ganesan, D. J. Ham and J. S. Lee, *Electrochem. Commun.,* 9 (2007), 2576-2579
17. J. P. Bosco, K. Sasaki, M. Sadakane, W. Ueda and J. G. Chen, *Chem. Mater.,* 22 (2010), 966-973
18. D. Chen, H. Wen, H. Zhai, H. Wang, X. Li, R. Zhang, J. Sun and L. Gao, *J. Am. Ceram. Soc.,* 93 (2010), 3997-4000
19. Y. Wang, S. Song, V. Maragou, P. K. Shen and P. Tsiakaras, *Appl. Catal. B: Environ.,* 89 (2009), 223-228
20. M. Wu, P. K. Shen, Z. Wei, S. Song and M. Nie, *J. Power Sources,* 166 (2007), 310-316
21. D. J. Ham, Y. K. Kim, S. H. Han and J. S. Lee, *Catal. Today,* 132 (2008), 117-122
22. G. He, Z. Yan, X. Ma, H. Meng, P. K. Shen and C. Wang, *Nanoscale,* 3 (2011), 3578
23. I.J. Hsu, D. A. Hansgen, B. E. McCandless, B. G. Willis and J. G. Chen, *J. Phys. Chem. C,* 115 (2011), 3709-3715
24. M. Shao, B. Merzougui, K. Shoemaker, L. Stolar, L. Protsailo, Z. J. Mellinger, I. J. Hsu and J. G. Chen, *J. Power Sources,* 196 (2011), 7426-7434
25. A.L. Stottlemyer, E. C. Weigert and J. G. Chen, *Ind. Eng. Chem. Res.,* 50 (2011), 16-22
26. M. Yin, Q. Li, J. O. Jensen, Y. Huang, L. N. Cleemann, N. J. Bjerrum and W. Xing, *J. Power Sources,* 219 (2012), 106-111
27. P. Ross Jr. and P. Stonehart, *J. Catal.,* 48 (1977), 42-59
28. Y. Hara, N. Minami and H. Itagaki, *Appl. Catal. A-Gen,* 323 (2007), 86-93
29. D. Ham, R. Ganesan and J. Lee, *Int. J. Hydrogen Energ.,* 33 (2008), 6865-6872
30. M. K. Hansen, D. Aili, E. Christensen, C. Pan, S. Eriksen, J. O. Jensen, J. H. von Barner, Q. Li and N. J. Bjerrum, *Int. J. Hydrogen Energ.* ,37 (2013), 10992-11000

31. H. Muroyama, K. Katsukawa, T. Matsui and K. Eguchi, *J. Electrochem. Soc.*, 158 (2011), B1072
32. J. B. Claridge, A. P. E., A. J. Brungs and M. L. H., *Chem. Mater.*, 12 (2000), 132-142
33. C. F. Davidson, G. B. Alexander and M. E. Wadsworth, *Metallurg. Trans. B*, 9 (1978), 553-557
34. Lide, Ed., Handbook of Chemistry and Physics, 86 Ed., CRC Press, 2005.
35. A.Kurlov and A. Gusev, *Inorg. Mater.*, 47 (2011), 133-138
36. F. H. Ribeiro, R. A. Dalla Betta, G. J. Guskey and M. Boudart, *Chem. Mater.*, 3 (1991), 805-812
37. V.Nikolova, I. Nikolov, T. Vitanov and L. Yotova, *J. Power Sources*, 12 (1984), 1-8
38. M. Neylon, S. Choi, H. Kwon, K. Curry and L. Thompson, *App. Catal. A-Gen.*, 183 (1999), 253-263
39. H. Chhina, S. Campbell and O. Kesler, , *J. Power Sources*, 179 (2008), 50-59
40. C. Brady, E. Rees and G. Burstein, *J. Power Sources* , 179 (2008), 17-26